JACS
JOURNAL OF THE AMERICAN CHEMICAL SOCIETY

ARTICLE

pubs.acs.org/JACS

Oligomerization State of Photosynthetic Core Complexes Is Correlated with the Dimerization Affinity of a Transmembrane Helix

Jen Hsin,[†,§] Loren M. LaPointe,[‡] Alla Kazy,[‡] Christophe Chipot,[*,†,∥] Alessandro Senes,[*,‡] and Klaus Schulten[*,†]

[†]Department of Physics and Beckman Institute for Advanced Science and Engineering, University of Illinois at Urbana−Champaign, Urbana, Illinois 61801, United States

[‡]Department of Biochemistry, University of Wisconsin−Madison, Madison, Wisconsin 53706, United States

Supporting Information

ABSTRACT: In the *Rhodobacter* (*Rba.*) species of photosynthetic purple bacteria, a single transmembrane α-helix, PufX, is found within the core complex, an essential photosynthetic macromolecular assembly that performs the absorption and the initial processing of light energy. Despite its structural simplicity, many unresolved questions surround PufX, the most important of which is its location within the photosynthetic core complex. One proposed placement of PufX is at the center of a core complex dimer, where two PufX helices associate in the membrane and form a homodimer. Inability for PufX of certain *Rba.* species to form a homodimer is thought to lead to monomeric core complexes. In the present study, we employ a combination of computational and experimental techniques to test the hypothesized homodimerization of PufX. We carry out a systematic investigation to measure the dimerization affinity of PufX from four *Rba.* species, *Rba. blasticus*, *Rba. capsulatus*, *Rba. sphaeroides*, and *Rba. veldkampii*, using a molecular dynamics-based free-energy method, as well as experimental TOXCAT assays. We found that the four PufX helices have substantially different dimerization affinities. Both computational and experimental techniques demonstrate that species with dimeric core complexes have PufX that can potentially form a homodimer, whereas the one species with monomeric core complexes has a PufX with little to no dimerization propensity. Our analysis of the helix−helix interface revealed a number of positions that may be important for PufX dimerization and the formation of a hydrogen-bond network between these GxxxG-containing helices. Our results suggest that the different oligomerization states of core complexes in various *Rba.* species can be attributed, among other factors, to the different propensity of its PufX helix to homodimerize.

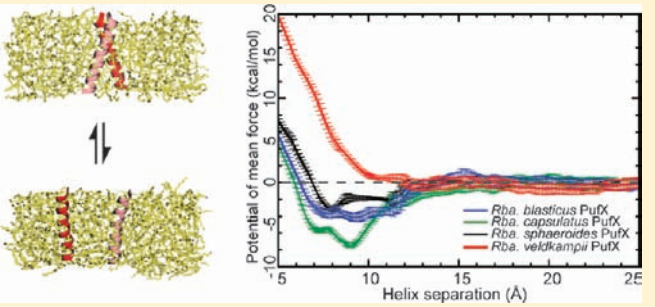

INTRODUCTION

Compared to algae and plants, bacterial photosynthesis, while similar in its chemical principles of energy conversion, is a lot simpler in the structure and organization of the associated protein−pigment assemblies. Nonetheless, there are many unknown features regarding the macromolecular arrangement of some of the most critical photosynthetic complexes, one example being the core complex of purple photosynthetic bacteria. The photosynthetic core complex is a combination of two major transmembrane (TM) protein−pigment complexes that carry out the initial steps of the photosynthetic process: light-harvesting complex 1 (LH1) and the reaction center (RC). In some species of purple bacteria, most notably the *Rhodobacter* (*Rba.*) genus, the core complex contains an additional TM protein that is largely α-helical and is named PufX for *Rhodobacters*. Some *Rhodobacter* core complexes can form dimers,[1,2] resulting in a large assembly with a dimension of approximately 20 nm × 10 nm in the membrane plane (Figure 1).[1,3−10]

The TM protein PufX is known to be crucial in the formation of dimeric photosynthetic core complexes in *Rba. sphaeroides*,[14] and deletion of this protein leads to monomeric core complexes.[2,9,15] Yet, as the location of PufX is still being debated, the molecular mechanism with which PufX determines the oligomerization state of the core complex is still an active topic of discussion.[15] Two models have been proposed for the placement and organization of PufX, each model involving a different mechanism for the PufX-assisted dimerization of the core complex (Figure 1). Figure 1a depicts a central placement of PufX, and the dimerization of the TM region of PufX "fuses" the two core complex monomers together.[4,6,16,17] In contrast, Figure 1b shows a placement of PufX near the gap of the two open LH1 rings,[7] and in this scheme PufX is thought to induce core complex dimerization via interaction of its long N-terminal region in the cytoplasmic space.[7,11,12] A crystallographic structure of a dimeric core complex is not yet available to determine unambiguously the validity of either model, although it has also been speculated that different species of *Rba.* bacteria might have different protein organizations in the core complex.[15,18]

Interestingly, the oligomerization states of different *Rba.* core complexes are not the same. Through atomic force microscopy (AFM) imaging of the *Rba. blasticus* photosynthetic membrane,

Received: May 26, 2011
Published: July 26, 2011

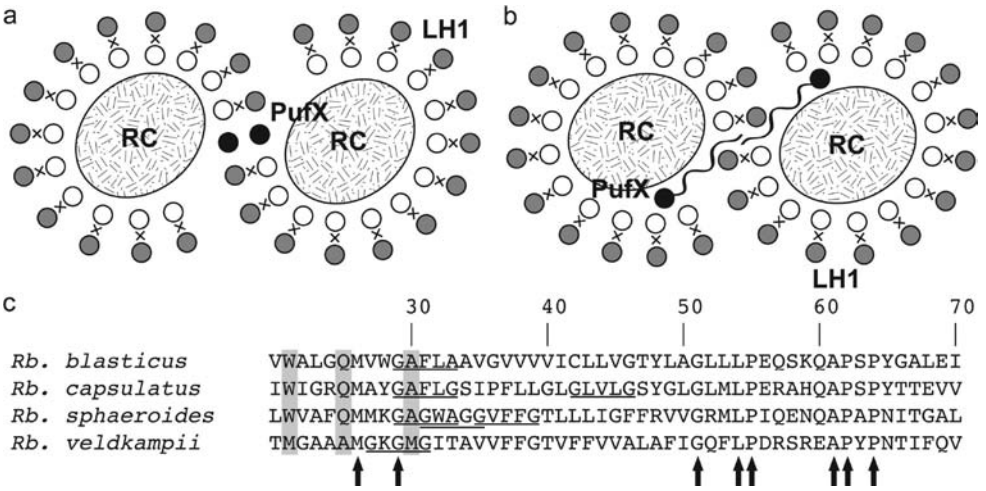

Figure 1. Proposed models for the protein organization of a dimeric photosynthetic core complex. (a) Model based on atomic force microscopy imaging studies of *Rba. sphaeroides* and *Rba. blasticus* photosynthetic membrane.[4,6] PufX is placed at the dimerization interface in the center of the core complex and is itself also thought to be dimerized. (b) Model based on the highest resolution structural data to date of the dimeric *Rba. sphaeroides* core complex,[7] with PufX situated near the gap of the open LH1 ring, and association of PufX is facilitated through a long loop at the N-terminal region.[7,11,12] In (a) and (b), PufX helices are represented by black circles, while LH1 helices are shown as gray circles (outer helices, known as LH1β) and white circles (inner helices, known as LH1α), with the embedded pigments between the outer and inner helices denoted by "X". RC is shown as an oval. (c) Aligned sequences of the central region of PufX from four *Rhodobacter* species investigated in the present study. Conserved amino acids are indicated by arrows, and amino acids conserved in *Rba. blasticus*, *Rba. capsulatus*, and *Rba. sphaeroides*, but not in *Rba. veldkampii*, are shaded in gray.[13] GxxxG and GxxxA motifs are underlined.

dimeric core complexes have been identified, although monomeric core complexes were also observed at an approximately 3:1 dimer to monomer ratio.[6] The *Rba. sphaeroides* core complex has also been shown to form dimers,[2,4,7,9] with monomeric core complexes present as well at a 1:1 dimer to monomer ratio.[18] Unlike *Rba. blasticus* and *Rba. sphaeroides*, the *Rba. veldkampii* core complex was observed to be monomeric in a structural and functional analysis,[19] and microscopy studies also reported no sighting of dimeric core complex in the *Rba. veldkampii* photosynthetic membrane,[13,17,20] suggesting that *Rba. veldkampii* core complex is unable to dimerize. While there is no structural information available for the *Rba. capsulatus* core complex, its PufX can replace that of *Rba. sphaeroides*, and the resulting *Rba. sphaeroides* is still photosynthetically viable,[15] prompting the idea that *Rba. sphaeroides* and *Rba. capsulatus* core complexes are likely very similar, and that the core complex of *Rba. capsulatus* is also capable of dimerizing.

Examining the sequences of PufX in four *Rba.* bacteria, it can be noted that some sequence similarities exist (Figure 1c).[13,15] In fact, it has been suggested that the GxxxG motif found in *Rba. sphaeroides* PufX between amino acids 31 and 35 (the N-terminal Met = 0 convention is adopted here) might serve as the dimerization region,[17,21] similar to that in glycophorin A (GpA).[22] Computational investigations have subsequently shown that a *Rba. sphaeroides* PufX dimer appears to be stable in a 1-palmitoyl-2-oleoyl-*sn*-glycero-3-phosphoethanolamine (POPE) membrane.[23] However, the GxxxG motif between locations 31 and 35 is only present in *Rba. sphaeroides*, not in *Rba. blasticus* or *Rba. capsulatus*, which also have a dimeric core complex. In addition, mutation of the glycines in this motif does not appear to abolish the ability for *Rba. sphaeroides* core complex to dimerize, as shown both computationally[23] and experimentally.[18] Furthermore, as shown in Figure 1c, GxxxG motifs are also present in *Rba. capsulatus* and *Rba. veldkampii*, although not between positions 31 and 35. A purely sequence-based argument for the dimerization affinity of PufX and the variability in core complex oligomerization state, thus, seems to be still inconclusive and requires further investigation.

In an effort to provide new insight into the potential dimerization of the PufX TM region, a prerequisite for the validity of the core complex organization shown in Figure 1a, and to relate dimerization of PufX segments to the core complex oligomerization state, we employed both computational and experimental methods to measure the dimerization affinity of four species of PufX: *Rba. blasticus*, *Rba. capsulatus*, *Rba. sphaeroides*, and *Rba. veldkampii*. We first constructed monomeric and dimeric PufX models for *Rba. blasticus*, *Rba. capsulatus*, and *Rba. veldkampii*, and then probed the stability of these structures in a membrane environment using all-atom molecular dynamics (MD), similar to the strategy previously followed for *Rba. sphaeroides* PufX.[23] Subsequently, TOXCAT[24] was performed on the four PufX TM segments to quantitatively measure the strength of helix−helix association. To complement the experiment, we also computed the apparent dimerization free energy for the four PufX helices using an MD-based free-energy protocol. Our data reveal a compelling trend on the strength of PufX dimerization: species capable of forming a dimeric core complex have PufX helices that show higher propensity to self-associate. Conversely, *Rba. veldkampii*, which is observed with only monomeric core complexes, has a PufX that exhibits very little propensity toward homodimerization. These results strongly indicate that differences in PufX dimerization affinity is an important factor for the variability of oligomerization states in *Rba.* photosynthetic core complexes.

METHODS

Molecular Dynamics. *Construction of Monomeric and Dimeric PufX.* As there are currently no structural data available for PufX from *Rba. blasticus*, *Rba. capsulatus*, and *Rba. veldkampii*, the monomeric PufX

models in simulations *blasticus-Monomer-POPE*, *capsulatus-Monomer-POPE*, and *veldkampii-Monomer-POPE* (Table 1) were constructed on the basis of that of *Rba. sphaeroides* PufX, for which two solution structures have been reported[11,21] and were used in previous modeling studies.[23,25−29] All PufX monomers were modeled with an integral TM helix with the same length as that of *Rba. sphaeroides* PufX.[21] Because we are only interested in the TM interaction of PufX helices, the N- and C-terminal residues that are thought to form loops[11,21] were not included. These monomeric PufX structures were then placed in a POPE membrane patch, with addition of neutralizing Na^+ and Cl^- ions at a total ionic strength of 300 mM, as shown in Figure 2a−c. For comparison, the *Rba. sphaeroides* PufX monomer, constructed previously,[23] is shown in Figure 2d.

Table 1. List of Molecular Dynamics Simulations Performed in the Present Study[a]

simulation name	type	number of atoms	time (ns)
blasticus-Monomer-POPE	EQ	32 812	15
capsulatus-Monomer-POPE	EQ	34 004	15
veldkampii-Monomer-POPE	EQ	32 904	15
blasticus-Dimer-POPE	EQ	31 801	50
capsulatus-Dimer-POPE	EQ	30 949	50
veldkampii-Dimer-POPE	EQ	32 336	100
blasticus-Dimer-DODE-1	EQ	20 486	10
capsulatus-Dimer-DODE-1	EQ	20 487	20
veldkampii-Dimer-DODE-1	EQ	20 557	10
blasticus-Dimer-DODE-ABF-1	ABF	20 486	220
capsulatus-Dimer-DODE-ABF-1	ABF	20 487	285
veldkampii-Dimer-DODE-ABF-1	ABF	20 557	185
blasticus-Dimer-DODE-2	EQ	20 496	20
capsulatus-Dimer-DODE-2	EQ	20 559	20
veldkampii-Dimer-DODE-2	EQ	20 503	20
blasticus-Dimer-DODE-ABF-2	ABF	20 496	55
capsulatus-Dimer-DODE-ABF-2	ABF	20 559	105
veldkampii-Dimer-DODE-ABF-2	ABF	20 503	70
sphaeroides-Dimer-DODE-ABF	ABF	20 584	170

[a] Total simulation time: 1.435 μs.

Equilibrium MD simulations were carried out for the three PufX monomer systems for 15 ns each. The final conformations of the PufX helices resulting from these monomer simulations were used to construct the corresponding PufX dimer models. Each PufX helix was replicated, and the two copies of PufX were placed facing each other by mapping them onto the GpA dimer structure,[22] as was previously done for *Rba. sphaeroides* PufX.[23] Because *Rba. blasticus*, *Rba. capsulatus*, and *Rba. veldkampii* do not have a GxxxG motif at position 31−35 (which *Rba. sphaeroides* possesses), amino acids 29−33 of *Rba. blasticus*, *Rba. capsulatus*, and *Rba. veldkampii* PufX were mapped onto the GxxxG portion of GpA. Choice of position 29−33 is based on the observation that *Rba. blasticus*, *Rba. capsulatus*, and *Rba. sphaeroides* all have a GxxxA or GxxxG motif at this segment, while *Rba. veldkampii* does not. In fact, Gly29 is conserved in all four species as shown in Figure 1c.

All PufX dimers were also placed in a POPE membrane patch, and similarly neutralized with additional ions at a total ionic strength of 300 mM, as shown in Figure 2e−g. The *Rba. sphaeroides* PufX dimer system[23] is shown in Figure 2h for comparison. An equilibrium MD simulation was performed for each of the resulting PufX dimer systems, designated as *blasticus-Dimer-POPE*, *capsulatus-Dimer-POPE*, and *veldkampii-Dimer-POPE* in Table 1, for at least 50 ns.

Equilibrium Molecular Dynamics. All simulations were performed using the MD package NAMD[30] with the CHARMM27 force field,[31,32]

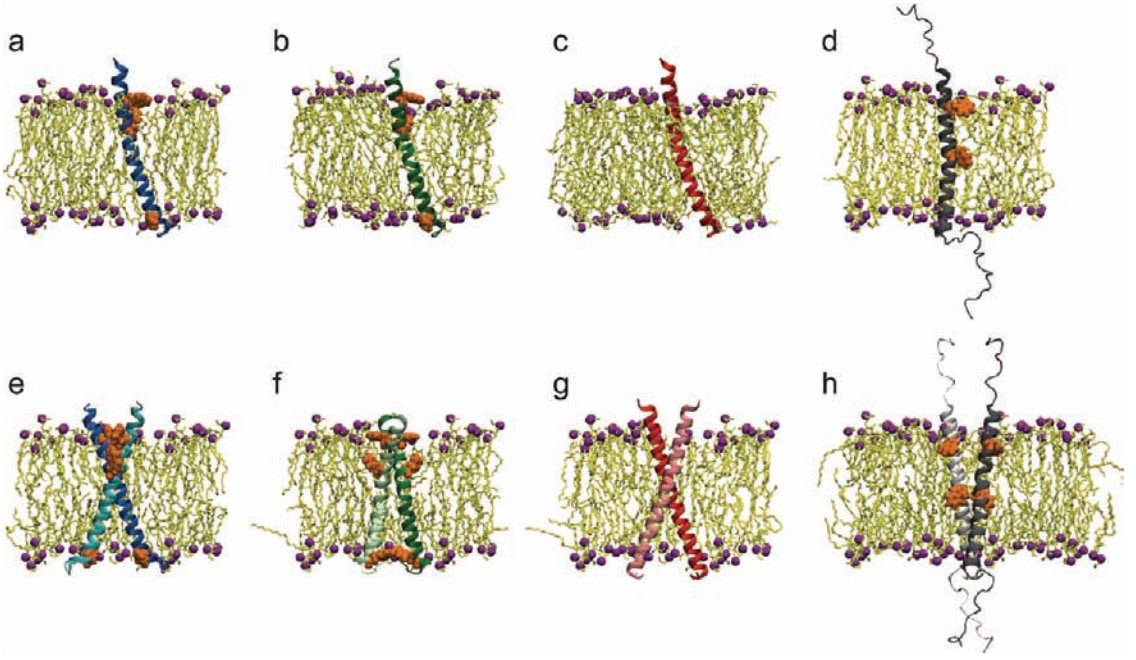

Figure 2. Simulated molecular systems with POPE lipid bilayers. Protein−membrane systems with monomeric PufX for (a) *Rba. blasticus*, (b) *Rba. capsulatus*, and (c) *Rba. veldkampii*. (d) Monomeric *Rba. sphaeroides* system is also shown for comparison; the simulation was performed previously.[23] PufX helix is shown in blue ((a) *Rba. blasticus*), green ((b) *Rba. capsulatus*), red ((c) *Rba. veldkampii*), and gray ((d) *Rba. sphaeroides*), lipid is shown in yellow with purple spheres representing the headgroups; polar-aromatic residues tyrosine and tryptophan of PufX are shown in orange. For clarity, water and ion molecules included in all simulations are not shown. (e−g) Protein−membrane systems with modeled homodimeric PufX for (e) *Rba. blasticus*, (f) *Rba. capsulatus*, and (g) *Rba. veldkampii*. (h) Dimeric *Rba. sphaeroides* system is also shown for comparison; the simulation was performed previously.[23] PufX helices in this and subsequent figures are shown with N-termini pointing upward.

including CMAP corrections.[33] Water molecules were described with the TIP3P model.[34] Long-range electrostatic forces were evaluated by means of the particle-mesh Ewald (PME) summation approach with a grid spacing of <1 Å. An integration time step of 2 fs was used in the framework of the Verlet r-RESPA algorithm.[35] Bonded terms and short-range, nonbonded terms were evaluated every time step, and long-range electrostatics was evaluated every other time step. Constant temperature (T = 310 K) was maintained using Langevin dynamics,[36] with a damping coefficient of 1.0 ps^{-1}. A constant pressure of 1 atm was enforced using the Langevin piston algorithm[37] with a decay period of 200 fs and a time constant of 50 fs.

Free-Energy Calculations. To assess computationally the dimerization affinity of the PufX helices, adaptive biasing force (ABF) calculations[38−40] were performed to determine free-energy as a function of helix−helix distance.[40,41] Prior to conducting ABF simulations, the PufX TM segments were equilibrated in a dodecane patch in a solvent environment neutralized with ions at 300 mM ionic strength. Use of dodecane as a lipid mimetic is dictated by the slow relaxation times of natural lipid molecules as compared to affordable MD time scales.[23,40,42] The TM segments of PufX were blocked at the N- and C-termini by Ac− and −NHMe groups, respectively. Two sets of PufX dimer−dodecane systems were constructed (*blasticus-Dimer-DODE-1*, *capsulatus-Dimer-DODE-1*, *veldkampii-Dimer-DODE-1*, *blasticus-Dimer-DODE-2*, *capsulatus-Dimer-DODE-2*, and *veldkampii-Dimer-DODE-2* in Table 1), using slightly different TM segments to test if inclusion of different residues would alter significantly the results of free-energy calculations. Each protein−dodecane system was subject to equilibrium MD for at least 10 ns. An example setup of the dodecan−PufX system is shown in Figure S1 in the Supporting Information.

ABF calculations were carried out subsequently in the framework of NAMD[30] for the six dodecane systems (*blasticus-Dimer-DODE-ABF-1*, *capsulatus-Dimer-DODE-ABF-1*, *veldkampii-Dimer-DODE-ABF-1*, *blasticus-Dimer-DODE-ABF-2*, *capsulatus-Dimer-DODE-ABF-2*, and *veldkampii-Dimer-DODE-ABF-2* in Table 1). The TM portion of a modeled *Rba. sphaeroides* PufX dimer was previously equilibrated in a dodecane patch,[23] and an ABF calculation was also performed for *Rba. sphaeroides* PufX, designated as *sphaeroides-Dimer-DODE-ABF* in Table 1. For each ABF simulation, the model reaction coordinate, ξ, is defined as the distance separating the center of mass of the two helices, in the interval 4.5 Å ≤ ξ ≤ 27 Å. A small ξ indicates that the PufX helices are associated, with a large ξ indicating their separation. In the course of an ABF simulation, average forces applied on the PufX helices in an unconstrained MD simulation are projected onto ξ, and a "biasing force" is calculated and applied to the helices to overcome local energy barriers.[38−40] The free-energy profile along ξ is then obtained by integrating the average force, with a standard error estimated according to Rodriguez-Gomez et al.[43]

TOXCAT. *Vectors and Constructs.* The TOXCAT vector, pccKAN, and positive controls containing the TM domain of wild type GpA (pccGpA-WT) and the G83I disruptive mutant (pccGpA-G83I) have been described previously.[24] DNA coding for the TM domains of the PufX proteins (Table 2), flanked by 5′NheI and 3′*Bam*HI restriction sequence, was purchased as synthetic genes (IDT). The sequences were ligated in-frame to *Nhe*I and *Bam*HI sites of the pccKAN vector.

Expression of ToxR′(TM)MBP Constructs. Plasmids encoding ToxR′-(TM)MBP chimerae were transformed into *Escherichia coli* MM39 cells (provided by D. M. Engelman) and plated onto Luria−Bertani (LB) plates (with 100 μg/mL ampicillin and 25 μg/mL streptomycin); colonies were inoculated into LB medium (with 100 μg/mL ampicillin) and stored as glycerol stocks at −80 °C. LB cultures (with 100 μg/mL ampicillin) were inoculated from frozen glycerol stocks and grown overnight (approximately 18 h). Three mL LB cultures (with 100 μg/mL ampicillin) were inoculated using 50 μL overnight cultures and grown to A_{420} 1.0, and 1 mL of cells was harvested by centrifugation and resuspended in 0.5 mL of lysis buffer (25 mM Tris-HCl, 2 mM EDTA, pH 8.0). Cells were then lysed by probe sonication. The lysate was clarified by centrifugation at 17 000g, and the supernatant was stored on ice until the spectrophotometric assay was performed.

Table 2. Sequences of the TM Regions of ToxR′(TM)MBP Constructs[a]

Species	Amino Acid Sequence
Rba. blasticus	**NRAS**QMVWGAFLAAVGVVVVICLLVGT**GIL**
Rba. capsulatus	**NRAS**QMAYGAFLGSIPFLLGLGLVLGS**GIL**
Rba. sphaeroides	**NRAS**QMMKGAGWAGGVFFGTKKKIGFF**GIL**
Rba. veldkampii	**NRAS**AMGKGMGITAVVFFGTVFFVVAL**GIL**

[a] Boldface residues represent the TOXCAT construct flanking regions including those containing the restriction site codons used for subcloning into the TOXCAT construct.

Spectrophotometric CAT Assay. The colorimetric assay used to detect chloramphenicol acetyltransferase activity in cell lysates was described previously.[44,45] Absorbance was measured using a PerkinElmer Lambda 25 UV/vis spectrophotometer. 40 μL of lysate was mixed with 1 mL of reaction buffer (0.1 mM acetyl-coA, 0.4 mg/mL 5,5′-dithiobis-(2-nitrobenzoic acid), 0.1 M Tris-HCl, pH 7.8), and absorbance at 412 nm was measured for a period of 2 min with intervals of 3 s to establish a basal rate of acetyl-coA hydrolysis in the absence of substrate. At 2 min, 40 μL of 2.5 mM chloramphenicol was added with mixing, and the absorbance was measured at 412 nm for another 2 min in 3 s intervals. CAT activity was calculated as the slope of 412 nm absorbance, after subtracting the basal rate prior to substrate addition. Lysates were assayed in triplicate, and the reported data are the result of three separate experiments.

Maltose Complementation Assays. To confirm correct membrane insertion, *E. coli* MM39 cells expressing the ToxR′(TM)MBP constructs were grown overnight in LB (with 100 μg/mL ampicillin) and then streaked onto M9 minimal media plates containing 0.4% maltose as the only carbon source and incubated for 3 days at 37 °C.

Western Blot Analysis. TOXCAT protein expression levels were verified by Western blot analysis. Cell lysate was mixed with 2× SDS-PAGE sample buffer, heated to 70 °C for 10 min, run on precast 12% polyacrylamide gels (Invitrogen), transferred onto an Immobilon-P polyvinylidene fluoride membrane (Millipore), and detected with rabbit anti-MPB primary antibodies (New England Biolabs) and antirabbit horseradish peroxidase conjugate secondary antibodies (Millipore).

RESULTS AND DISCUSSION

Below, our computational and experimental results are discussed. First, we report the stability of different species of PufX helices in monomeric and homodimeric conformations as probed by equilibrium MD simulations. Next, we present the dimerization affinity of PufX helices as measured using the TOXCAT assay. Finally, complementing TOXCAT experiments with atomic resolution and quantitative assessment, we report MD-based free-energy calculations conducted to estimate the apparent dimerization free energy, ΔG_{app}, of PufX helices.

Equilibrium Molecular Dynamics. *PufX Monomers.* All three PufX monomers were seen to be structurally stable during their respective equilibrium MD simulations. Similar to *Rba. sphaeroides*, the PufX helices of *Rba. blasticus*, *Rba. capsulatus*, and *Rba. veldkampii* were seen to tilt with respect to the normal of the lipid bilayer during simulations (see movies S1a, S1b, and S1c in the Supporting Information). Examining the sequence content of PufX from the different species, it was observed that *Rba. veldkampii* is the only case without either a tyrosine or a tryptophan residue. Tyrosine and tryptophan residues are known

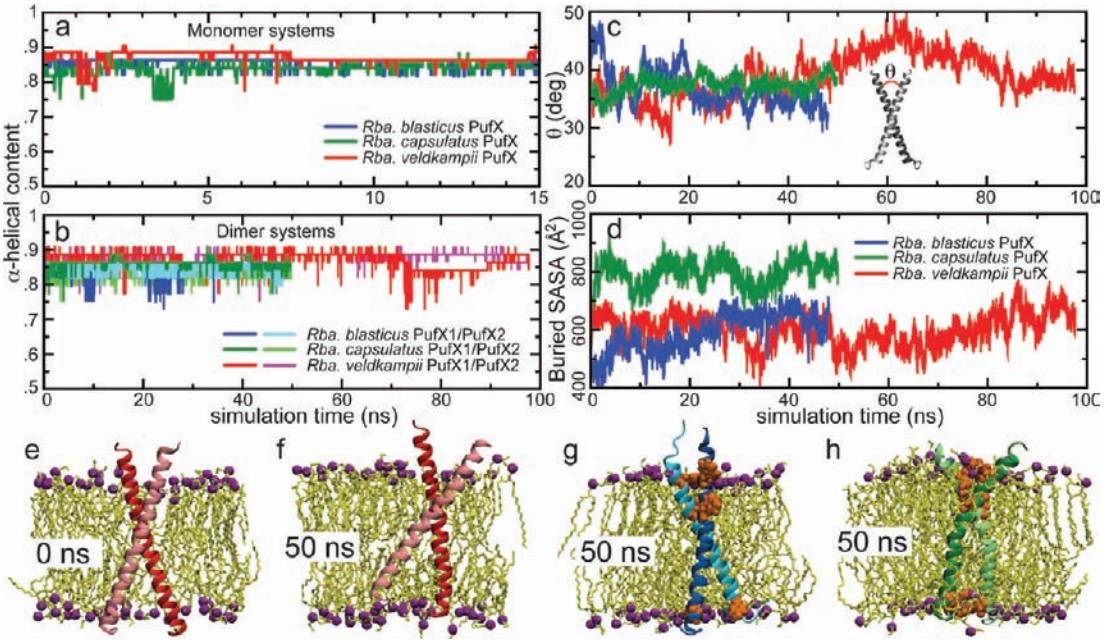

Figure 3. Stability of PufX monomeric and homodimeric helices during equilibrium MD simulations. (a) α-Helical content of the modeled PufX monomer in a full POPE membrane. For each of the three species tested (*Rba. blasticus*, *Rba. capsulatus*, and *Rba. veldkampii*), PufX retains its high α-helical content. Similarly, modeled PufX helices in dimeric conformation also remain largely α-helical, as shown in (b). (c) Crossing-angle between the dimerized helices. (d) Buried solvent-accessible surface area (SASA) as a measure for helix−helix interaction. Parts (e) and (f) show the movement of the *Rba. veldkampii* PufX helices. At 50 ns, one of the *Rba. veldkampii* helices can be seen to submerge nearly fully into the membrane on the C-terminus. For comparison, (g) and (h) show the *Rba. blasticus* and *Rba. capsulatus* PufX helices also at 50 ns; in these cases, the tyrosine and tryptophan residues aided in anchoring the helices in the membrane, and these residues remained at the membrane−solvent interface throughout the simulation.

to reside preferentially at the lipid−water interface[46] and might contribute to the anchoring of a TM helix to the lipid headgroups.[47−49] As can be seen in Figure 2a−d, for *Rba. blasticus*, *Rba. capsulatus*, and *Rba. sphaeroides* PufX that contain tyrosine and tryptophan, most of these residues appear near the membrane−solvent interface.

The helical structures of all PufX models persisted throughout the simulations, as shown in Figure 3a. Structural stability of each PufX monomer is consistent with the two-stage model of membrane−protein folding, which postulates that TM helices act as independent stable domains and are preformed prior to their association into large protein complexes[50,51]

PufX Dimers. Each PufX dimer model was constructed using the final conformation from the equilibrium simulations of monomeric PufX, as described in the Methods. All three dimer systems were observed to be structurally robust with consistent α-helical content throughout the simulation (Figure 3b; see movies S2a, S2b, and S2c in the Supporting Information). The dimerized PufX helices also maintained a consistent crossing-angle (Figure 3c) and remained in contact during the simulation as indicated by the measurement of the buried solvent-accessible surface area (SASA) (Figure 3d). For all three species, buried SASA of the PufX dimers remained near or above 600 Å^2, comparable to that of GpA.[52]

The most notable motion was seen in the case of *Rba. veldkampii* PufX, which lacks both tyrosine and tryptophan, and transformed from an originally upright orientation (Figure 3e) to one tilted relative to the membrane at 50 ns (Figure 3f), and with one of the helices submerged in the lipid phase on the C-terminus. This tilted and partially membrane-buried conformation of the *Rba. veldkampii* PufX dimer persisted when the simulation was extended to 100 ns. In comparison, the tyrosine and tryptophan residues in *Rba. blasticus* and *Rba. capsulatus* PufX dimers (Figure 3g and h, respectively) remained at the membrane−solvent interface, preventing strong fluctuations in their helix−membrane orientations. Quantitative measurement of helix tilting with respect to the membrane normal during the simulations *blasticus-Dimer-POPE*, *capsulatus-Dimer-POPE*, and *veldkampii-Dimer-POPE* is shown in Figure S2 in the Supporting Information. The instability of *Rba. veldkampii* PufX helices due to the lack of anchorage might be significant in the propensity of the helices to homodimerize. Additionally, it can be seen that the proline residue at position 36 in *Rba. capsulatus* PufX induces a moderate kink in the helix (10−30°) that persisted throughout the simulations for both the mononeric and the dimeric conformations (Figure S3); this residue does not face the dimerization interface in the modeled *Rba. capsulatus* PufX dimer.

Interhelical interactions contributing to the stability of PufX dimer models are shown in Figure 4a−c for *Rba. blasticus*, *Rba. capsulatus*, and *Rba. veldkampii*, respectively. For *Rba. blasticus* and *Rba. capsulatus*, significant molecular interactions are contributed by residues Gln25 and Met26, which interact with each other, and also with other small amino acids such as glycine and alanine. For example, Gln25 was seen to interact with Ala22, and Met26 interacted with Gly29 in *Rba. blasticus* PufX dimer (Figure 4a). The Met26−Gly29 interaction was also observed for *Rba. capsulatus*, and its Gln25 was observed to interact with Ile22 (Figure 4b). Also, helix packing is achieved through close contact between small residues Gly29 and Ala30 for both *Rba. blasticus* and *Rba. capsulatus* (Figure 4a and b). Notably, while Gly29 is conserved for all four species investigated in the present

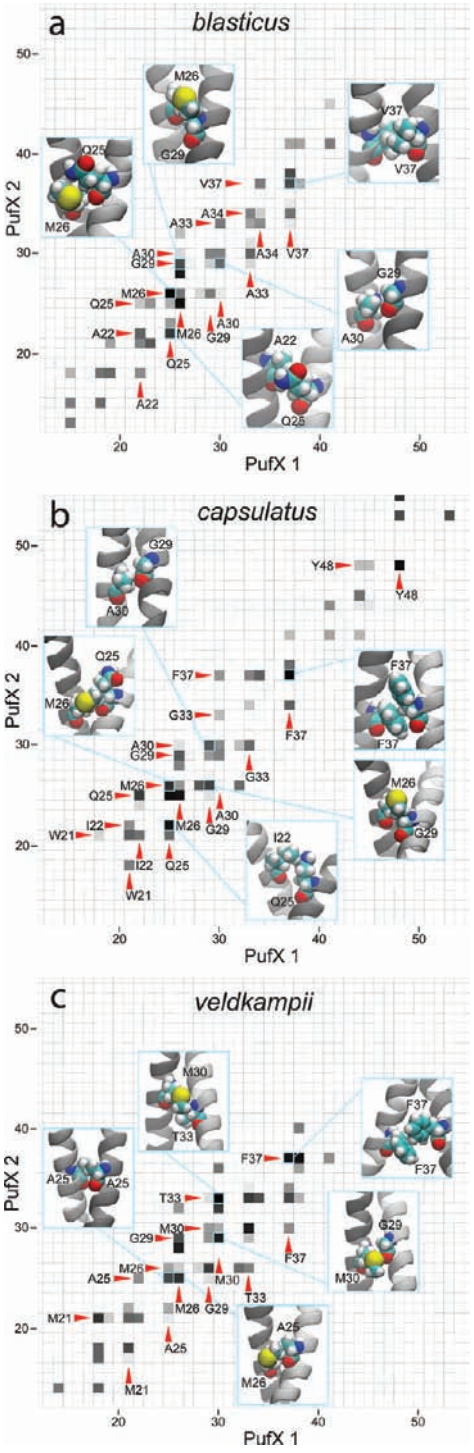

Figure 4. Interhelical interactions observed during the equilibrium molecular dynamics simulations (a) *blasticus-Dimer-POPE*, (b) *capsulatus-Dimer-POPE*, and (c) *veldkampii-Dimer-POPE*. In each interaction map, highly interacting amino acid pairs are highlighted with darker grids, and five of such pairs are shown in the insets as examples.

study, *Rba. veldkampii* is the only species that does not contain Gln25 and Ala30 (Figure 1c), two residues that contribute significantly to interhelical interactions for *Rba. blasticus* and *Rba. capsulatus*. For *Rba. veldkampii* PufX dimer, the helices are held together by a slightly different set of molecular interactions, although Met26, which is conserved in all four PufX sequences

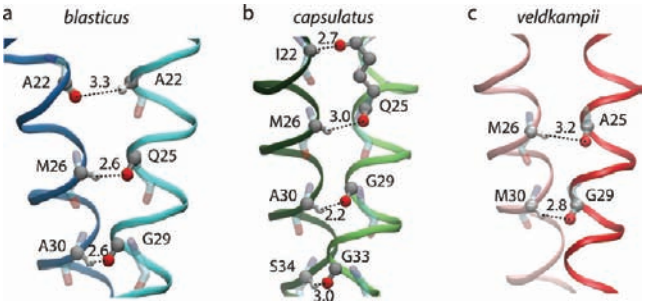

Figure 5. Networks of interhelical C_α—H···O hydrogen-bond contacts in the three PufX dimer models identified from simulations (a) *blasticus-Dimer-POPE*, (b) *capsulatus-Dimer-POPE*, and (c) *veldkampii-Dimer-POPE*. For the amino acids involved in formation of C_α—H···O contacts, carbon atoms are shown in gray, oxygen atoms in red, hydrogen atoms in white, and other backbone atoms are shown in transparent. All H···O distances are shown in angstroms.

(Figure 1c), plays also an important role (Figure 4c). Further away from the dimerization core, bulkier amino acids such as Val37 for *Rba. blasticus*, and Phe37 for *Rba. capsulatus* and *Rba. veldkampii*, provide additional interhelix contact.

Interhelical hydrogen bonds are known to be an important factor in mediating helix—helix association in the membrane.[53] The close packing of the modeled PufX dimers permitted the formation of several interhelical hydrogen bonds. In particular, the side-chain amide group of Gln25 forms an interhelical hydrogen bond with the carbonyl of Ala22 in the *Rba. blasticus* dimer (Figure 5). The same side chain accepts a C_α—H···O hydrogen bond from Ile22 in the *Rba. capsulatus* dimer. As mentioned above, *Rba. veldkampii* is the only species that does not contain Gln25. Several backbone-to-backbone C_α—H···O hydrogen bonds were also observed (illustrated in Figure 5 and Table 3), which are a hallmark of GxxxG-mediated transmembrane interactions.[53−58] The Gln25—Met26 and Gly29—Ala30 pairs were seen to be sites for the potential formation of C_α—H···O hydrogen bonds for the cases of *Rba. blasticus* and *Rba. capsulatus* PufX dimers, and locations 33 and 34, which contain small amino acids such as alanine, serine, and glycine, provide additional hydrogen bonding (Figure 5 and Table 3). For the case of *Rba. veldkampii* PufX dimer, only two C_α—H···O hydrogen bonds were observed and were also formed between amino acid pairs 25—26 (Ala25—Met26) and 29—30 (Gly29—Met30).

TOXCAT. The equilibrium MD simulations of the three PufX dimers conducted here, as well as the one conducted previously for *Rba. sphaeroides*,[23] showed that PufX dimer models for all four species remain associated. Although it appears that the *Rba. veldkampii* PufX dimer has an unstable protein—membrane interaction due to the lack of anchorage, no spontaneous disassociation was observed. It is possible that disassociation of PufX requires longer simulation time than is currently feasible due to the slow relaxation time of a full POPE membrane.

To determine quantitatively the dimerization affinity of the PufX helices, we employed an experimental assay, the TOXCAT method,[24] which measures the association of TM helices in a biological membrane. Three TOXCAT measurements were performed on each of the four *Rba.* species, with the average dimerization affinity for each species shown in Figure 6b as percent of the CAT activity of GpA. *Rba. capsulatus* is seen to have the highest propensity for homodimerization, with a relative

Table 3. Geometry of Potential $C_\alpha-H\cdots O$ Hydrogen-Bond Contacts[a]

donor	acceptor	d_H (min value)	d (min value)	ζ	ξ	θ
		Ideal Values				
		≤2.7	≤3.8	180	120	0
		Rba. blasticus				
A22	A22	4.04 (3.03)	4.75 (3.75)	127.06	103.68	28.11
M26	Q25	3.65 (2.54)	4.42 (3.42)	131.82	85.87	29.44
A30	G29	3.06 (2.78)	3.83 (3.13)	129.28	96.57	17.14
A34	A33	3.90 (2.76)	4.69 (3.66)	132.64	96.42	39.62
		Rba. capsulatus				
I22	Q25	3.01 (2.20)	4.03 (3.27)	158.92	110.55	54.45
M26	Q25	2.86 (2.24)	3.80 (3.14)	146.67	120.92	61.52
A30	G29	2.97 (2.21)	3.56 (3.01)	115.23	108.14	15.58
S34	G33	4.79 (2.81)	5.58 (3.80)	133.70	115.98	38.84
		Rba. veldkampii				
M26	A25	2.61 (2.14)	3.51 (3.07)	141.31	115.86	46.91
M30	G29	2.82 (2.17)	3.65 (3.11)	135.74	104.27	13.96

[a] Definitions of distances and angles are given as the following:[54,57] d_H is the distance between the H and O atoms; d is the distance between the C_α and the O atoms; ζ is the $C_\alpha-H-O$ angle; ξ is the $H-O-C$ angle; and θ is the elevation angle between the $C_\alpha-H$ vector and the amide plane. All numbers are average values from the last 10 ns of corresponding simulations (*blasticus-Dimer-POPE*, *capsulatus-Dimer-POPE*, and *veldkampii-Dimer-POPE*). Distances are given in angstroms, and angles are given in degrees.

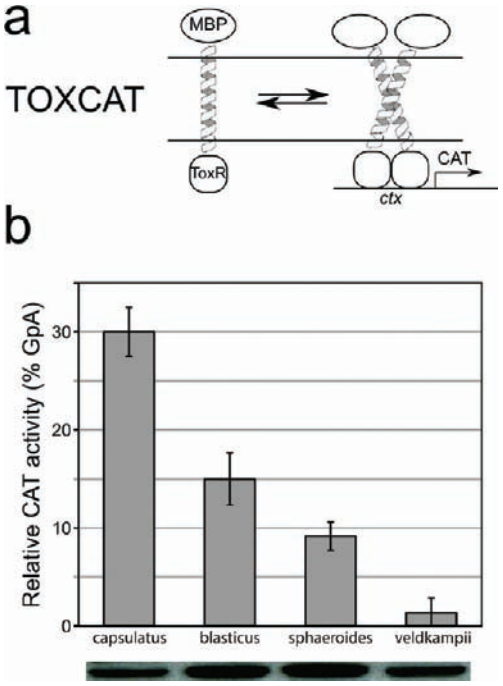

Figure 6. Quantification of association of TM constructs in *E. coli* membranes using TOXCAT. (a) TOXCAT[24] is an in vivo assay based on a fusion construct consisting of the TM domain under investigation, a maltose binding protein, and the ToxR transcriptional activator of *V. cholerae*. TM association results in the expression of chloramphenicol acetyl transferase (CAT) under the ctx promoter, whose enzymatic activity can be measured. (b) TOXCAT data for the PufX TM domains of *Rba. capsulatus*, *Rba. blasticus*, *Rba. sphaeroides*, and *Rba. veldkampii*. The data are reported as percent of the CAT activity of GpA, a strongly dimerizing transmembrane domain.[22] The data are the average of three independent measurements, and the error bars report the standard deviation. Protein expression levels were verified by Western blot using anti-MBP antibodies.

CAT activity at ∼30%, comparable to a prior measurement reported in Aklujkar and Beatty.[59] *Rba. blasticus* has the second highest CAT activity, albeit only at ∼15% GpA. *Rba. sphaeroides* shows even lower propensity to homodimerize, and *Rba. veldkampii* exhibits no significant CAT activity.

Free-Energy Calculations. Concurrent to the experimental measurement of PufX dimerization affinity with TOXCAT, we also employed free-energy calculations to measure the apparent dimerization free energy in silico using the ABF algorithm[38−40] for PufX from four *Rba*. species. The computational treatment is inspired by the atomic resolution of the method, which can reveal great structural details in the dimerization and disassociation pathway.

Two sets of ABF calculations were conducted corresponding to distinct choices of TM residues. In the first set, the same sequences as those used in TOXCAT (i.e., those shown in nonboldface in Table 2) were included. Because the TOXCAT experiments contain also flanking residues and are not identical to the setup of the in silico assays, to test if results from ABF are sensitive to the small difference in the sequence of amino acids, a second set of ABF simulations was conducted, using the sequences identified as the TM region from the dimer simulations carried out in the POPE environment (i.e., *blasticus-Monomer-POPE*, *capsulatus-Monomer-POPE*, and *veldkampii-Monomer-POPE*; Table 1). For *Rba. sphaeroides* PufX, the sequence used in TOXCAT is the same as that identified as the TM region;[23] therefore, only one ABF simulation was performed (*sphaeroides-Dimer-DODE-ABF* in Table 1).

The dimerization pathway of PufX is observed to be more complex than that of GpA,[40] with an example shown in Figure 7 for the case of *Rba. sphaeroides* PufX. At the beginning of the ABF simulation *sphaeroides-Dimer-DODE-ABF*, the two PufX helices are both straight (Figure 7a). However, spontaneous bending occurred after 13 ns (Figure 7b, left), in agreement with prior in silico observation on the inherent flexibility of the *Rba. sphaeroides* PufX helix.[23] Furthermore, bending of the PufX helix occurs at the same location as that seen for one of the PufX solution structures,[11] and, as a result, the bent conformation seen in simulation *sphaeroides-Dimer-DODE-ABF* is structurally very similar to the solution structure (Figure 7b, right). Helix bending persisted for a few tens of a nanosecond, but eventually the helix spontaneously straightened (Figure 7c). Previously, we had estimated that bending of the *Rba. sphaeroides* PufX only costs a few kcal/mol;[23] our present results support such a low value. We note that the tendency for *Rba. sphaeroides* PufX to bend might complicate self-association, but does not completely prohibit it as the helix quickly straightens back and the straight conformation can possibly be stabilized by dimerization.

The results from the two sets of ABF calculations are compared in Figure 8 in the form of free-energy profiles as a function of helix−helix distance. For the first set of ABF calculations (Figure 8a), all four species of PufX are seen to have energy minima for an associated, dimerized conformation, albeit with different well depths. *Rba. veldkampii* has the most shallow free-energy minimum near a helix−helix separation of 12 Å. *Rba. sphaeroides* has the second-most shallow free-energy minimum.

Unlike the GpA dimer, which exhibits a well-defined free-energy well,[40] the free-energy well of *Rba. sphaeroides* PufX is seen to span nearly 5 Å, with the minimum occurring near 8 Å. *Rba. blasticus* and *Rba. capsulatus* have the deepest free-energy wells, and both possess multiple local minima. For *Rba. capsulatus*, two local free-energy minima are found at helix−helix distances of 8 and 11 Å; for *Rba. blasticus*, its free-energy well has several less well-defined local minima that stretch up to a helix−helix distance of 15 Å. The much wider free-energy well for *Rba. blasticus* PufX is possibly due to additional stabilizing interhelical interactions arising from transient van der Waals contact between the bulkier Leu43, Leu44, and Thr47 residues near the C-terminal end (Figure S4 in the Supporting Information). In general, the PufX dimers exhibit more complex free-energy profiles than does the GpA dimer.[40] This extra complexity is possibly due to the usage of modeled dimer systems rather than experimentally derived structures. Alternatively, it is also possible that the complex dimerization scheme is intrinsic to PufX due to its difference to GpA.

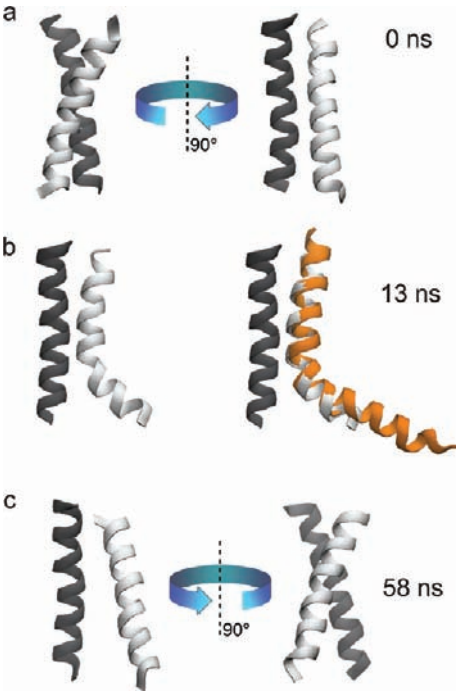

Figure 7. Spontaneous bending and straightening of *Rba. sphaeroides* PufX. (a) At the onset of the ABF simulation for *Rba. sphaeroides* PufX, both helices were straight. (b) At 13 ns, one of the helices bent spontaneously. The bending corresponded well to the observed NMR solution structure of PufX (pdb code 2NRG[11]) and persisted for the next ~40 ns. (c) The bent helix was seen to straighten back at 58 ns, suggesting that bending and straightening of the helix occur spontaneously with a low energy barrier, as suggested previously.[23]

In the second set of ABF simulations (Figure 8b), *Rba. veldkampii* appears to have no preference for association. *Rba. capsulatus* PufX is seen to have a deeper free-energy well than that of *Rba. blasticus* and retains the two minima observed in Figure 8a, albeit at closer helix−helix distances (7 and 9 Å). *Rba. blasticus* PufX again exhibits a wide minimum, with the global free-energy minimum occurring at a helix−helix distance of 9 Å. Although the precise free-energy profiles are different in the two sets of ABF simulations, it is reassuring that distinct features in the *Rba. blasticus* and *Rba. capsulatus* free-energy profiles are preserved across the two simulations. Additionally, *Rba. veldkampii* PufX consistently exhibits the lowest propensity toward dimerization.

From the free-energy profiles in Figure 8, we calculated the apparent disassociation free energy, ΔG_{app}, for the four species of PufX in two sets of ABF calculations using the expression utilized by Hénin et al.,[40] with the results shown in Table 4 and Figure 9. Calculation of ΔG_{app} allows comparison of PufX dimerization affinity with that of GpA (Figure 9), which has a ΔG_{app} value of 11.5 ± 0.4 kcal/mol as previously reported using also the ABF method in a dodecane environment.[40] It can be seen that the order of PufX dimerization affinity is similar to the experimental results (Figure 6), in the decreasing order of *Rba. capsulatus* > *Rba. blasticus* > *Rba. sphaeroides* > *Rba. veldkampii*. Differences in

Table 4. Free Energy of Association[a]

species	ΔG_{app} from ABF1 (kcal/mol)	ΔG_{app} from ABF2 (kcal/mol)
Rba. capsulatus	6.7 ± 0.3	9.4 ± 0.3
Rba. blasticus	6.8 ± 0.4	6.6 ± 0.5
Rba. sphaeroides	5.2 ± 0.4	n/a
Rba. veldkampii	3.8 ± 0.3	0

[a] Two ABF calculations were conducted each for *Rba. blasticus*, *Rba. capsulatus*, and *Rba. veldkampii* PufX segments using slightly different amino acid sequences (Figure 8), and one ABF calculation was performed for *Rba. sphaeroides*.

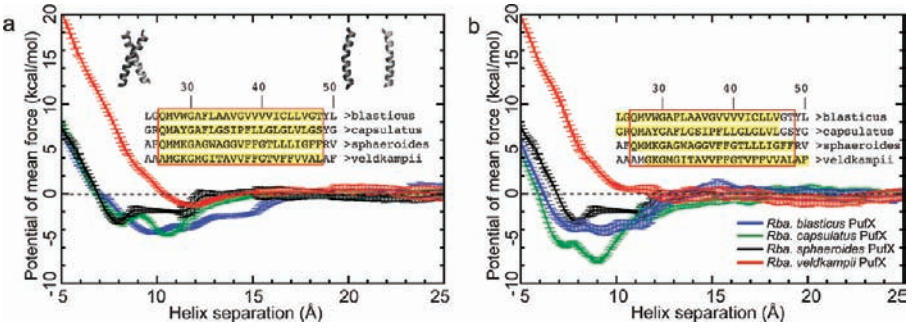

Figure 8. Potential of mean force measured in ABF simulations. Highlighted sequences are those included in the ABF simulations; the sequences outlined in the red box are those included in the TOXCAT measurement (Table 2). (a) First set of ABF simulations using the same sequence for TM segments of PufX as that in TOXCAT experiments. (b) Second set of ABF simulations using the sequence identified as the TM segments in the PufX dimer−POPE membrane simulations.

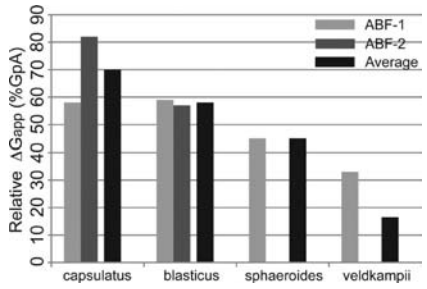

Figure 9. Free energy of association, ΔG_{app}, for various PufX sequences as a fraction of GpA ΔG_{app}. GpA ΔG_{app} was calculated in Hénin et al.[40]

experimental and simulation setups might contribute to the consistent overestimate of in silico free energies as compared to TOXCAT measurements (Figures 9 and 6). For example, the PufX sequences used in the TOXCAT experiment and the ABF measurements are not exactly identical (Table 2 and Figure 8), and, as shown by comparing Figure 8a and b, small differences in sequence content can lead to varying dimerization affinity. Additionally, while TOXCAT was performed in a biological membrane environment, the ABF measurements were conducted with dodecane. Finally, the reaction coordinate, ξ, chosen in the ABF calculation does not consider the relative orientation of the two helices, including their intrinsic rotation about their longitudinal axis, a degree of freedom important in optimizing helix−helix packing. Considering these factors limiting direct comparison between experiment and simulation results, it is significant that a consensus in the relative strength of dimerization for the four PufX sequences tested here was reached.

CONCLUDING REMARKS

We have shown through experiments and molecular dynamics simulations that PufX from different *Rba.* species of purple photosynthetic bacteria exhibit distinct propensities toward homodimerization. This result can explain in part why core complexes have different oligomerization states in different species, namely, due to the different inherent affinity of the TM regions of PufX to dimerize. In particular, species with PufX shown to be least likely to dimerize, *Rba. veldkampii*, form only monomeric core complexes.[13,17] On the other hand, *Rba. blasticus* that possesses dimeric core complexes[6] is seen to have PufX with a relatively high dimerization affinity.

In addition to the ability for dimerization at the TM region, the presence of aromatic amino acids with polar groups (tyrosine and tryptophan) appears to aid in stabilizing PufX helices in the membrane. *Rba. veldkampii* PufX contains no tyrosine or tryptophan and also shows the lowest tendency for dimerization in its TM region. These two characteristics of *Rba. veldkampii* PufX, the lack of anchoring residues and a TM region with low likelihood for self-association, make *Rba. veldkampii* PufX a poor candidate for forming homodimers. Interestingly, a tryptophan residue on the N-terminal end of the TM region is part of the recently identified PufX motif that is missing in *Rba. veldkampii*, but present in *Rba. blasticus*, *Rba. capsulatus*, and *Rba. sphaeroides* (Figure 1c).[13]

While *Rba. blasticus*, *Rba. capsulatus*, and *Rba. sphaeroides* PufX show some preference for self-association, their dimerization affinity is significantly lower than that of GpA.[52,60] The lower dimerization affinity might be the reason why dimeric and monomeric core complexes are both present in *Rba. blasticus* and *Rba. sphaeroides*,[4,6,18] as a subset of PufX helices might be in monomeric forms in the photosynthetic membrane, residing in monomeric core complexes. It is also possible that dimerization of PufX requires additional molecular interactions other than those arising from the PufX TM region, or between PufX and the rest of the core complex. For *Rba. sphaeroides*, there are experimental reports showing that the N-terminal segment of PufX is critical for the formation of dimeric core complexes,[12,61] although the molecular role of these residues in PufX-assisted core complex dimerization is unclear. Dimerization of PufX might also be strengthened by interaction between PufX and LH1α helices observed previously for *Rba. sphaeroides* and *Rba. capsulatus*,[62] or by the binding of the light-absorbing pigment bacteriochlorophyll (shown in Figure 1a and b as crosses) to PufX.[59,63,64] Speculation that different *Rba.* species might have different organizations for their core complexes has also been raised.[15,18]

While identification of a GxxxG motif in the *Rba. sphaeroides* PufX sequence at the 31−35 position is intriguing,[17,21] the motif by itself does not explain the observed oligomerization states of *Rba.* core complexes. As alluded to above, *Rba. blasticus* lacks this particular sequence motif, yet it has been confirmed to contain dimeric core complexes.[6] It should be noted, however, that *Rba. blasticus*, *Rba. capsulatus*, and *Rba. sphaeroides* actually all feature a GxxxA/G motif at the 29−33 position that is not present in *Rba. veldkampii* (Figure 1c), with GxxxA previously suggested as a motif for dimerization of TM helices.[55,65−69] The glycine residue at position 29 in PufX is actually conserved across the four *Rba.* species, and an alanine residue is found at position 30 except for *Rba. veldkampii* PufX (Figure 1c), providing another small amino acid that allows for potential helix−helix interaction. It is conceivable that the combination of presence of protein−membrane anchoring provided by tyrosine or tryptophan, and small amino acids such as glycine and alanine at the helix−helix contact site, renders a PufX TM segment more prone to homodimerize.

ASSOCIATED CONTENT

Supporting Information. Complete citation for ref 31, six movies, seven additional figures, and one table. This material is available free of charge via the Internet at http://pubs.acs.org.

AUTHOR INFORMATION

Corresponding Author

chipot@ks.uiuc.edu; senes@wisc.edu; kschulte@ks.uiuc.edu

Present Addresses

[§]Department of Bioengineering, Stanford University, Stanford, California 94305, United States.

[∥]Equipe de Dynamique des Assemblages Membranaires, UMR Centre National de la Recherche Scientifique/UHP 7565, Nancy Université BP 239, Nancy, France.

ACKNOWLEDGMENT

We thank C. Neil Hunter and Pu Qian for many helpful discussions, Simon Scheuring for illuminating communications, and Ben Mueller for assistance in performing the TOXCAT assays. This work was supported by Grants NSF MCB-0744057 and NIH P41-RR005969. Computer time was provided by

NCSA and TACC via Large Resources Allocation Committee Grant MCA93S028, resources of the Argonne Leadership Computing Facility at Argonne National Laboratory, supported by the Office of Science of the U.S. Department of Energy (Contract DE-AC02-06CH11357), and resources of the Oak Ridge Leadership Computing Facility at Oak Ridge National Laboratory, which is supported by the Office of Science of the U.S. Department of Energy under Contract DE-AC05-00OR22725.

REFERENCES

(1) Jungas, C.; Ranck, J.-L.; Rigaud, J.-L.; Joliot, P.; Verméglio, A. *EMBO J.* **1999**, *18*, 534–542.
(2) Siebert, C. A.; Qian, P.; Fotiadis, D.; Engel, A.; Hunter, C. N.; Bullough, P. A. *EMBO J.* **2004**, *23*, 690–700.
(3) Loach, P. A. *Proc. Natl. Acad. Sci. U.S.A.* **2000**, *97*, 5016–5018.
(4) Scheuring, S.; Francia, F.; Busselez, J.; Melandris, B. A.; Rigaud, J.-L.; Lévy, D. *J. Biol. Chem.* **2004**, *279*, 3620–3626.
(5) Scheuring, S.; Lévy, D.; Rigaud, J.-L. *Biochim. Biophys. Acta* **2005**, *1712*, 109–127.
(6) Scheuring, S.; Busselez, J.; Lévy, D. *J. Biol. Chem.* **2005**, *280*, 1426–1431.
(7) Qian, P.; Hunter, C. N.; Bullough, P. A. *J. Mol. Biol.* **2005**, *349*, 948–960.
(8) Cogdell, R. J.; Gall, A.; Köhler, J. *Q. Rev. Biophys.* **2006**, *39*, 227–324.
(9) Qian, P.; Bullough, P. A.; Hunter, C. N. *J. Biol. Chem.* **2008**, *283*, 14002–14011.
(10) Scheuring, S.; Sturgis, J. N. *Photosynth. Res.* **2009**, *102*, 197–211.
(11) Tunnicliffe, R. B.; Ratcliffe, E. C.; Hunter, C. N.; Williamson, M. P. *FEBS Lett.* **2006**, *580*, 6967–6971.
(12) Ratcliffe, E. C.; Tunnicliffe, R. B.; Ng, I. W.; Adams, P. G.; Qian, P.; Holden-Dye, K.; Jones, M. R.; Williamson, M. P.; Hunter, C. N. *Biochim. Biophys. Acta* **2011**, *1807*, 95–107.
(13) Liu, L.-N.; Sturgis, J. N.; Scheuring, S. *J. Struct. Biol.* **2011**, *173*, 138–145.
(14) Francia, F.; Wang, J.; Venturoli, G.; Melandri, B. A.; Barz, W. P.; Oesterhelt, D. *Biochemistry* **1999**, *38*, 6834–6845.
(15) Holden-Dye, K.; Crouch, L. I.; Jones, M. R. *Biochim. Biophys. Acta* **2008**, *1777*, 613–630.
(16) Scheuring, S. *Curr. Opin. Cell Biol.* **2006**, *10*, 387–393.
(17) Busselez, J.; Cottevielle, M.; Cuniasse, P.; Gubellini, F.; Boisset, N.; Lévy, D. *Structure* **2007**, *15*, 1674–1683.
(18) Crouch, L. I.; Holden-Dye, K.; Jones, M. R. *Biochim. Biophys. Acta* **2010**, *1797*, 1812–1819.
(19) Gubellini, F.; Francia, F.; Busselez, J.; Venturoli, G.; Lévy, D. *Biochemistry* **2006**, *45*, 10512–10520.
(20) Milhiet, P.-E.; Gubellini, F.; Berquand, A.; Dosset, P.; Rigaud, J.-L.; Le Grimellec, C.; Lévy, D. *Biophys. J.* **2006**, *91*, 3268–3275.
(21) Wang, Z.-Y.; Suzuki, H.; Kobayashi, M.; Nozawa, T. *Biochemistry* **2007**, *46*, 3635–3642.
(22) MacKenzie, K. R.; Prestegard, J. H.; Engelman, D. M. *Science* **1997**, *276*, 131–133.
(23) Hsin, J.; Chipot, C.; Schulten, K. *J. Am. Chem. Soc.* **2009**, *131*, 17096–17098.
(24) Russ, W. P.; Engelman, D. M. *Proc. Natl. Acad. Sci. U.S.A.* **1999**, *96*, 863–868.
(25) Chandler, D.; Hsin, J.; Harrison, C. B.; Gumbart, J.; Schulten, K. *Biophys. J.* **2008**, *95*, 2822–2836.
(26) Hsin, J.; Gumbart, J.; Trabuco, L. G.; Villa, E.; Qian, P.; Hunter, C. N.; Schulten, K. *Biophys. J.* **2009**, *97*, 321–329.
(27) Sener, M. K.; Hsin, J.; Trabuco, L. G.; Villa, E.; Qian, P.; Hunter, C. N.; Schulten, K. *Chem. Phys.* **2009**, *357*, 188–197.
(28) Hsin, J.; Chandler, D. E.; Gumbart, J.; Harrison, C. B.; Sener, M.; Strumpfer, J.; Schulten, K. *ChemPhysChem* **2010**, *11*, 1154–1159.
(29) Trabuco, L. G.; Schreiner, E.; Gumbart, J.; Hsin, J.; Villa, E.; Schulten, K. *J. Struct. Biol.* **2011**, *173*, 420–427.
(30) Phillips, J. C.; Braun, R.; Wang, W.; Gumbart, J.; Tajkhorshid, E.; Villa, E.; Chipot, C.; Skeel, R. D.; Kale, L.; Schulten, K. *J. Comput. Chem.* **2005**, *26*, 1781–1802.
(31) MacKerell, A. D., Jr.; Bashford, D.; Bellott, M.; Dunbrack, R. L., Jr.; Evanseck, J. D.; Field, M. J.; Fischer, S.; Gao, J.; Guo, H.; Ha, S.; Joseph-McCarthy, D.; Kuchnir, L.; Kuczera, K.; Lau, F. T. K.; Mattos, C.; et al. *J. Phys. Chem. B* **1998**, *102*, 3586–3616.
(32) Foloppe, N.; MacKerell, A. D., Jr. *J. Comput. Chem.* **2000**, *21*, 86–104.
(33) MacKerell, A. D., Jr.; Feig, M.; Brooks, C. L., III. *J. Comput. Chem.* **2004**, *25*, 1400–1415.
(34) Jorgensen, W. L.; Chandrasekhar, J.; Madura, J. D.; Impey, R. W.; Klein, M. L. *J. Chem. Phys.* **1983**, *79*, 926–935.
(35) Tuckerman, M. E.; Berne, B. J.; Martyna, G. J. *J. Phys. Chem. B* **1992**, *97*, 1990–2001.
(36) Brünger, A. T.; Brooks, C. L., III; Karplus, M. *Chem. Phys. Lett.* **1984**, *105*, 495–500.
(37) Feller, S. E.; Zhang, Y.; Pastor, R. W.; Brooks, B. R. *J. Chem. Phys.* **1995**, *103*, 4613–4621.
(38) Darve, E.; Pohorille, A. *J. Chem. Phys.* **2001**, *115*, 9169–9183.
(39) Hénin, J.; Chipot, C. *J. Chem. Phys.* **2004**, *121*, 2904–2914.
(40) Hénin, J.; Pohorille, A.; Chipot, C. *J. Am. Chem. Soc.* **2005**, *127*, 8478–8484.
(41) Kim, H.; Hsin, J.; Liu, Y.; Selvin, P. R.; Schulten, K. *Structure* **2010**, *18*, 1443–1449.
(42) Stockner, T.; Ash, W. L.; MacCallum, J. L.; Tieleman, D. P. *Biophys. J.* **2004**, *87*, 1650–1656.
(43) Rodriguez-Gomez, D.; Darve, E.; Pohorille, A. *J. Chem. Phys.* **2004**, *120*, 3563–3578.
(44) Shaw, W. V. *Methods Enzymol.* **1975**, *43*, 737–755.
(45) Sulistijo, E. S.; Jaszewski, T. M.; MacKenzie, K. M. *J. Biol. Chem.* **2003**, *278*, 51950–51956.
(46) Senes, A.; Chadi, D. C.; Law, P. B.; Walters, R. F. S.; Nanda, V.; DeGrado, W. F. *J. Mol. Biol.* **2007**, *366*, 436–448.
(47) Killian, J. A.; von Heijne, G. *Trends Biochem. Sci.* **2000**, *25*, 429–434.
(48) Yuen, C. T. K.; Davidson, A. R.; Deber, C. M. *Biochemistry* **2000**, *39*, 16155–16162.
(49) de Planque, M. R. R.; Killian, J. A. *Mol. Membr. Biol.* **2003**, *20*, 271–284.
(50) Popot, J.-L.; Engelman, D. M. *Biochemistry* **1990**, *29*, 4031–4037.
(51) Engelman, D. M.; Chen, Y.; Chin, C.-N.; Curran, A. R.; Dixon, A. M.; Dupuy, A. D.; Lee, A. S.; Lehnert, U.; Matthews, E. E.; Reshetnyak, Y. K.; Senes, A.; Popot, J.-L. *FEBS Lett.* **2003**, *555*, 122–125.
(52) Fleming, K. G.; Ackerman, A. L.; Engelman, D. M. *J. Mol. Biol.* **1997**, *272*, 266–275.
(53) Bowie, J. U. *Curr. Opin. Struct. Biol.* **2011**, *21*, 42–49.
(54) Senes, A.; Ubarretxena-Belandia, I.; Engelman, D. M. *Proc. Natl. Acad. Sci. U.S.A.* **2001**, *98*, 9056–9061.
(55) Senes, A.; Engel, D. E.; DeGrado, W. F. *Curr. Opin. Struct. Biol.* **2004**, *14*, 465–479.
(56) Arbely, E.; Arkin, I. T. *J. Am. Chem. Soc.* **2004**, *126*, 5362–5363.
(57) Derewenda, Z. S.; Lee, L.; Derewenda, U. *J. Mol. Biol.* **1995**, *252*, 248–262.
(58) Lawrie, C. M.; Sulistijo, E. S.; MacKenzie, K. R. *J. Mol. Biol.* **2010**, *396*, 924–936.
(59) Aklujkar, M.; Beatty, J. T. *Photosynth. Res.* **2006**, *88*, 159–171.
(60) Duong, M. T.; Jaszewski, T. M.; Fleming, K. G.; MacKenzie, K. R. *J. Mol. Biol.* **2007**, *371*, 422–434.
(61) Francia, F.; Wang, J.; Zischka, H.; Venturoli, G.; Oesterhelt, D. *Eur. J. Biochem.* **2002**, *269*, 1877–1885.
(62) Recchia, P. A.; Davis, C. M.; Lilburn, T. G.; Beatty, J. T.; Parkes-Loach, P. S.; Hunter, C. N.; Loach, P. A. *Biochemistry* **1998**, *37*, 11055–11063.
(63) Parkes-Loach, P. S.; Law, C. J.; Recchia, P. A.; Kehoe, J.; Nehrlich, S.; Chen, J.; Loach, P. A. *Biochemistry* **2001**, *40*, 5593–5601.
(64) Law, C. J.; Chen, J.; Parkes-Loach, P. S.; Loach, P. A. *Photosynth. Res.* **2003**, *75*, 193–210.

(65) Senes, A.; Gerstein, M.; Engelman, D. M. *J. Mol. Biol.* **2000**, *296*, 921–936.
(66) Schneider, D. *FEBS Lett.* **2004**, *577*, 5–8.
(67) Schneider, D.; Engelman, D. M. *J. Mol. Biol.* **2004**, *343*, 799–804.
(68) Kairys, V.; Gilson, M. K.; Luy, B. *Eur. J. Biochem.* **2004**, *271*, 2086–2092.
(69) Rath, A.; Deber, C. M. *Proteins: Struct., Funct., Bioinf.* **2008**, *70*, 786–793.